Postprint of: Pęczkowski P., Łuszczek M., Szostak E., Muniraju N.K.C., Krztoń-Maziopa A., Gondek Ł., Superconductivity and appearance of negative magnetocaloric effect in $Ba_{1-x}K_xBiO_3$ perovskites, doped by Y, La and Pr, ACTA MATERIALIA, Vol. 222, (2022), 117437, DOI: 10.1016/j.actamat.2021.117437

Superconductivity and appearance of negative magnetocaloric effect in $Ba_{1-x}K_xBiO_3$ perovskites, doped by Y, La and Pr

Paweł Pęczkowski[1,2,*], Maciej Łuszczek[3], Elżbieta Szostak[4], Naveen Kumar Chogondahalli Muniraju[2,5], Anna Krztoń-Maziopa[6], Łukasz Gondek[5]

[1] Institute of Physical Sciences, Faculty of Mathematics and Natural Sciences, School of Exact Sciences, Cardinal Stefan Wyszyński University, K. Wóycickiego 1/3 Street, 01-938 Warsaw, Poland

[2] Institute of Solid State Physics, TU Wien, Wiedner Hauptstraße 8-10 Street, 1040 Vienna, Austria

[3] Faculty of Electrical and Control Engineering, Gdańsk University of Technology, Gabriela Narutowicza 11/12 Street, 80-233 Gdańsk, Poland

[4] Faculty of Chemistry, Jagiellonian University, Gronostajowa 2 Street, 30-387 Kraków, Poland

[5] Department of Solid State Physics, Faculty of Physics and Applied Computer Science, AGH University of Science and Technology, A. Mickiewicza 30 Avenue, 30-059 Kraków, Poland

[6] Faculty of Chemistry, Warsaw University of Technology, S. Noakowskiego 3 Street, 00-664 Warsaw, Poland

* Corresponding author: P. Pęczkowski, p.peczkowski@uksw.edu.pl, p.peczkowski@wp.pl

Abstract

Recently, substantial attention is given to the bismuth-based perovskites for variety of electronic applications. The perovskites are used for quantum dots displays (QLED), photovoltaic systems and superconducting (HTS) devices. In this paper comprehensive studies of $Ba_{1-x}K_xBi_{1-y}RE_yO_3$ bismuth perovskites (REBKBO, RE = Y, La or Pr) are reported. Apart from structural anomalous behavior at low temperatures, the electronic properties of the REBKBO can be easily tailored by doping. For instance, critical current densities differ by 3 orders of magnitude from 0.07 kA/cm^2 (LaBKBO) to 65 kA/cm^2 (BKBO). To explain the above behavior, microstructural, magnetic, calorimetric, spectroscopic (FT-IR) studies and ab-initio electronic structure calculations were carried out. The FT-IR shows that the biggest difference in the spectrum compared to the undoped sample was recorded for PrBKBO, due to magnetic contribution of the Pr^{3+} multiplet. Electronic structure calculations revealed that the BKBO compound shows the highest DOS(E_F) compared to the other samples, however, the electronic structure of PrBKBO is very different. The negative magnetocaloric effect observed below 30 K is a highlight of the peculiar properties of that sample. These findings extend possible usage of bismuth-based perovskites towards new applications.

Keywords: *Copper-free oxide high-T_c superconductors; Magnetic properties*; *Spectroscopic measurements*; *Microstructure*; *Density Functional Theory*

1. Introduction

High-temperature superconductivity (HTS) attracts scientists attention in many fields ranging from HTS magnets, quantum superconducting devices, energetics, biomedicine, etc. Since its discovery in 1986 by Bednorz and Müller, new materials with significantly higher critical temperatures have been discovered [1-3]. For copper-based superconductors it is possible to move the critical temperature above 160 K for Hg-based cuprates at high pressures [4].

Research on HTS is still an emerging field of material science and solid state physics. The critical temperatures of 203 K for H_2S at 100 GPa [5] and 287 K for H_2S with CH_4 at 267 GPa [6] were recently discovered. Apparently, HTS in those compounds does not rely on Cu–O planes. Therefore, research on copper-free HTS is an essential field as concerns our understanding of physics standing behind this phenomenon. In 1975 the $BaPb_{0.7}Bi_{0.3}O_3$ with a critical temperature of $T_c \sim 13$ K was discovered [7]. Next, the $Ba_{1-x}K_xBiO_3$ ($x \sim 0.40$) the so-called BKBO, was discovered in 1988 year [8,9]. This was the first copper-free oxide superconductor with a critical temperature above 30 K, which is higher than the critical temperature of the best intermetallic superconductor [10,11]. BKBO materials are easily synthetized by conventional ceramic technique by mixing $BaCO_3$, Bi_2O_3, KO_2 precursors in appropriate proportions, and then annealing them at 993 K in argon and then at 693 K in oxygen [10,12]. A single crystal of the BKBO superconductor can also be obtained by electrocrystallization from a mixture of molten hydroxides [13].

The crystal structure and transport properties of the $Ba_{1-x}K_xBiO_3$ perovskite depend on the potassium K content [10,12]. $Ba_{1-x}K_xBiO_3$ at the room temperature has a monoclinic distorted structure of the perovskite with the $I2/m$ space group for $x = 0$. For $0.15 < x \leq 0.35$, the monoclinic phase is transformed into the orthorhombic $Ibmm$ phase, and then for $x > 0.35$ into the cubic $Pm\bar{3}m$ structure. The cubic to orthorhombic transition is temperature

dependent and may occur for $0.10 < x < 0.37$. The transport properties of BKBO change from semiconducting to metallic for potassium content $x > 0.35$. Superconductivity occurs only in the cubic phase near $x = 0.40$ and disappears with an increase in $x > 0.50$ [12]. Optimal conditions for the growth of superconducting and non-conductive single crystals and layers with a given chemical composition and dependence on the critical temperature (T_c), lattice parameters and coefficients of thermal expansion in $Ba_{l-x}K_xBi0_3$ with different potassium content are discussed in Refs. Barilo et al. [14], and Klinkova et al. [15].

C. Yajing et al. [16] in their work synthesized the $Ba_{0.6-x}RE_xK_{0.4}BiO_3$ (RE = La, Pr) system for $x = 0$, 0.025, 0.05, 0.1, 0.2, 0.3; 0.4, using the molten salt method. In order to obtain the best homogeneity, the ratio Bi^{3+}/Bi^{5+} was assumed to be 0.8357. Samples were characterized using the X-ray diffraction (XRD) method and by measuring the temperature dependences of magnetization. The influence of rare earth doping on the crystal structure and superconductivity of the $Ba_{0.6-x}Pr_xK_{0.4}BiO_3$ system was examined showing that for $x = 0$, there is a quasi-regular structure, which for $x = 0.025$, 0.05 and 0.1 changes into a transitional orthorhombic structure, and at higher $x = 0.2$, 0.3, and 0.4, an extended quasi-regular structure appears accompanied by gradual changes of the crystal lattice. The structural distortion and the associated lattice expansion can be explained by replacement of smaller Bi^{5+} with a slightly larger Pr^{4+} or a larger Pr^{3+} . The contraction of the crystal lattice is associated with the substitution of larger Ba^{2+} or Bi^{3+} by smaller Pr^{4+} or Pr^{3+} . Therefore, the anisotropic changes in the axial dimensions and the resulting change of the quasi-regular to orthorhombic structure can be interpreted as a result of the simultaneous replacement of some Ba and Bi ions by Pr ions. It has been found that T_c is suppressed at relatively low dopant contents with $x \leq 0.1$ and disappears when $x \leq 0.4$. The radius of the Pr cations is smaller than that of the Ba cations, which results in enhancing the octahedral distortion, and leads to charge disproportionation and suppression of superconductivity. Substitution of Pr^{4+} in the Bi^{5+} position significantly

increased the distortion of the crystal structure and the disproportionation of the charge in the $Ba_{0.6}K_{0.4}BiO_3$ system with the Pr dopant. The reason for the attenuation of T_c is therefore the distortion of the crystal structure caused by the oxidation state of the substituted ion and its radius. For La and Y doped samples similar relations were observed. The crystal lattice of the system contracts because both La^{3+} and Y^{3+} cations are smaller than Ba^{2+} and K^{+}, while they are larger than Bi^{3+} and Bi^{5+}. Therefore, it can be concluded that the shrinkage of the crystal lattice is consistent with the substitution at Ba site. T_c is suppressed also at low dopant contents $x \leq 0.1$ and disappears at $x \leq 0.2$ [16,17].

It has been shown that for $x \in (0.375; 0.40)$ T_c changes without apparent correlation to potassium content in the sample. This proves that the substitution of potassium for barium is not the only factor responsible for the properties of the obtained superconducting material [18-20]. The superconducting and optical properties of bismuth perovskites result from the overlapping of the Bi-6*s* and O-2*p* valence bands in BiO_6 octahedrons [21,22]. The influence of oxygen stoichiometry on the valence state of a metal occurs not only in the case of bismuth perovskites [23], but also in the case of BiSrCaCuO cuprates [24] and thin layers of oxygen-doped halides [25]. The relationship between the Bi and O valence states in $Ba_{1-x}K_xBiO_3$ (BKBO) perovskites and their properties in the superconducting state was also discussed in the literature [26].

The perovskite structure of the BKBO excludes the existence of a two-dimensional metal-oxygen sublayer, which could be analogous to the CuO_2 planes responsible for superconductivity in copper-oxygen superconductors. In BKBO no magnetic ordering was observed [27], and the magnetic susceptibility is typical of Pauli paramagnet [28,29]. Therefore, it is commonly believed that the electron-phonon (EP) interaction is responsible for the origin of superconductivity in BKBO [30]. The macroscopic EP interactions in BKBO were investigated using a realistic structure of the $BaBiO_3$ electron band and discussed in the

papers by L.F. Mattheiss and D.R. Hamann [31,32]. The superconducting properties of BKBO, such as T_c, isotope effect, superconducting energy gap and tunneling spectra, have been studied in detail based on the strong coupling theory developed by Eliashberg [33,34].

Today, many questions remain open, including those about the correlation between superconducting properties of BKBO and: electronic structure, nature of chemical bonds, magnetic, transport and optical properties.

There is also another field of interest in BKBO compounds. The (111) oriented $BaBiO_3$ two-layer structure, sandwiched between the large-gap perovskite oxides, is similar to that of graphene [35]. Therefore, it is an ideal candidates for topological electronics that uses topological charges as degrees of freedom to electric current conduction. These graphene-like electronic structures, due to the numerous Dirac cones and the π-Berry phase of each Dirac cone, provide the ideal platform that researchers are currently focusing on interests. [36,37].

In our contribution we report and discuss the results of microstructural, structural, magnetic and calorimetric studies of $Ba_{0.63}K_{0.37}BiO_3$ and $RE_yBa_{1-x}K_xBi_{1-y}O_3$ (RE is Y, La or Pr) compounds. To get a deeper insight into origins of the observed properties DFT (Density Functional Theory) calculations were also provided.

2. Experimental

2.1. Synthesis and preparation of samples

In 1989, Norton [13] discovered the electrochemical technique of low temperature crystallization, which he developed in 1991 with Tang [37]. In 1989, the synthesis was carried out in the KOH flux at the temperature of 260 °C in a three-electrode single-chamber chamber. It is the best and most economical method of producing BKBO crystals and BKBO with partial substitutions with rare elements RE such as La, Y, Pr. The synthesis method provides sample of better quality than the conventional ceramic method, in which BKBO was

first synthesized by Cava et al. [8]. The samples produced by the electrochemical process exhibit higher T_c and greater homogeneity of the monocrystalline superconducting phase. Also, using this method, Nishio et al. [38] obtained large single crystals of $Ba_{1-x}K_xBiO_3$. The reaction that takes place during this process can be described by the chemical equation:

$$9Ba(OH)_2 \cdot 8H_2O + 11Bi_2O_3 + 6KOH \rightarrow 15Ba_{0.6}K_{0.4}BiO_3 + 7Bi_{(metal)} + 84H_2O$$

The design of the Norton and Tang [37] electrochemical synthesis cells included a teflon (PTFE: Polytetrafluoroethylene) reaction cell and a quartz holder for three electrodes. The potentiostatic deposition was performed using a three-electrode single-chamber cuvette geometry. The working electrode (positive or anodically polarized) can be Ag or Pt. The counter electrode (negative or polarized cathode) was only Pt. The reference electrode was a 1 cm long Bi rod, reactive and stable in diameter (~ 0.5 mm). The reference electrode was placed close to the working electrode. The slow rise based on the low current density (0.5 mA/cm^2) at the working electrode produces a more uniform superconducting single crystal phase, but the optimal rise time and current density remain uncertain [39]. It was found that both K^+/Ba^{2+} and K^+/Bi^{3+} are significant factors influencing the production of the homogeneous BKBO phase [40].

The synthesis time is limited by the depletion of Ba_2O_3 from the alloy by depositing the bimetal on the counter electrode (cathode) and the mixed valence of Bi on the working electrode (anode). The superconducting properties of BKBO depend on the percentage of Ba and K. The transition to the superconducting phase, from T_c ~ 32 K, takes place in about 38% ÷ 39% of K. As K increases, the superconducting transition temperature slowly decreases until the ratio of 50% K : 50% Ba is obtained. The BKBO compound becomes a semiconductor for K > 50%. In the case of $Ba_{0.6}K_{0.4}BiO_3$, the percentage of Bi^{3+} is 30% and

Bi^{5+} is 70%. Increasing the Bi^{5+} percentage in BKBO drives the K_2O component upwards, from $BaBiO_3$ to $KBiO_3$ [37].

Nevertheless, the kinetic and thermodynamic processes of BKBO electrocrystallization in the KOH flux are still not fully known [41], which results in heterogeneity of the obtained samples. Many researchers have tried to fine-tune this process to obtain more homogeneous materials. The goal of these studies was to obtain single crystals of the superconducting phase of this compound and to determine the structure of the desired phase by single crystal X-ray diffraction [42,43].

The synthesis of the REBKBO samples for RE = Y, La, Pr were done by electrocrystallization in teflon crucible equipped with two platinum electrodes, at current density of 10 mA/cm^2 and temperature 245°C. $Ba(OH)_2 \cdot 8H_2O$, Bi_2O_3, KOH and selected rare earth oxides were used in appropriate molar ratios as substrates for preparation of reaction mixtures. Crystals were grown on anodically polarized electrode, and after 72 hours extracted from the hot melt, washed repeatedly with distilled water and acetone, dried and kept in sealed vessels. Details can be found in our previous paper [26].

2.2. Methods

Microstructure and energy-dispersive X-ray spectroscopy (EDS) studies were made using JEOL 5900 LV scanning electron microscope (SEM). The specimens were characterized by X-ray diffraction, as well, by means of Panalytical Empyrean powder diffractometer with Cu Kα radiation source. The measurements were done using the Bragg-Brentano geometry on finely powdered samples. The samples were powdered in an agate mortar. Fractions used for measurements were separated using 10 μm sieve. For low-temperature studies (15 ÷ 300 K) PheniX helium close-cycle refrigerator by Oxford Instruments was used. The sample position was corrected automatically against thermal

displacement. Obtained diffraction patterns were refined using Rietveld-type FullProf software [44].

The magnetization and specific heat measurements were performed using a Vibrating Sample Magnetometer, (VSM, Quantum Design Physical Property Measurement System - PPMS 9T). The measurements were performed as a function of temperature at fixed magnetic field $M(T)$, or as a function of magnetic field while temperature kept stable $M(H)$. Before each $M(H)$ measurement the sample was cooled from above T_c in the absence of magnetic field. The specific heat measurements were made in the 0 and 8 T field range.

The FT-IR (Fourier-Transform Infrared Spectroscopy) measurements were performed using a Bruker VERTEX 70v Fourier transform infrared spectrometer. Spectra were collected over the range 400 ÷ 4000 cm^{-1} with a resolution of 2 cm^{-1}. The samples have been admixed with KBr and pelletized by pressing under sufficient pressure, before FT-IR analysis. An Advanced Research System (ARS) helium DE-202A cryostat and water-cooled helium ARS-2HW compressor working in a closed cycle manner, with controlled heating and cooling rates and temperature stabilization within ±0.2 °C, were used to obtain the spectra at low temperatures. The temperature of the „cold finger" was measured with an accuracy of ±1 °C.

IR spectrum analysis were carried out according to standard procedure (peak position analyzing) and using OPUS Software. Temperature-dependent IR spectra of the samples were compared by cluster analysis [45]. For cluster analysis, the second derivation of the vector normalized spectra were used for calculation with Ward's algorithm (OPUS 7.0) [46].

In this work Quantum ESPRESSO (QE) program was employed for the first-principles electronic structure calculations in the framework of Density Functional Theory (DFT) [47, 48]. The examined REBKBO compounds were modelled by 2x2x2 supercells with eight $BaBiO_3$ unit cells taken as an initial crystal structure. In the as-prepared 40-atom supercell

three Ba atoms and one Bi atom were replaced by three K atoms and one RE atom (RE = Y, La, Pr), respectively, to obtain $Ba_{0.625}K_{0.375}Bi_{0.875}RE_{0.125}O_3$ system with the stoichiometry, which is very close to the experimental one. As a reference, the BKBO supercell, containing no rare-earth atom ($Ba_{0.625}K_{0.375}BiO_3$), was constructed. All calculations were carried out utilizing Perdew-Burke-Ernzerhof (PBE) version of pseudopotentials and using 4x4x4 k-point mesh for the Brillouin zone sampling. The applied kinetic energy (charge density) cut-off was 60 Ry (480 Ry). In the case of strongly correlated Pr 4*f* electrons the on-site Coulomb interaction was taken into account using the Hubbard parameter U = 6 eV (DFT + U method) to improve the calculations. The geometry optimization of the supercells was performed by fitting total energy vs. cell volume curves to the Birch-Murnaghan equation of state (EOS) to find the minimum. The positions of atoms were relaxed until the on-site forces were less than 10^{-3} Ry/a.u. The electronic structure calculations were performed for the evaluated theoretical lattice constants, which were as follows: 4.34528 Å (BKBO), 4.33028 Å (YBKBO), 4.36405 Å (LaBKBO) and 4.32289 Å (PrBKBO). To make the analysis of density of states (DOS) more reliable, the Gaussian smearing with 0.001 Ry width was applied.

3 Results and discussion

3.1. Microstructure and chemical microanalysis

The synthesized compounds exhibit surprisingly different morphologies. The microstructure of investigated compounds with X-ray microanalysis maps of elements' distribution is depicted in the Figure 1. As apparent, in the $Ba_{0.6}K_{0.4}Bi_{0.88}Y_{0.12}O_3$ a needle-like crystallite shape with broad size distribution can be seen. On the other hand, for $Ba_{0.63}K_{0.37}BiO_3$ and $Ba_{0.55}K_{0.45}Bi_{0.87}Pr_{0.13}O_3$ rather bulky cube-like crystallite shapes were evidenced. For $Ba_{0.59}K_{0.41}Bi_{0.87}La_{0.13}O_3$ another behavior was observed. Namely, the large crystallites are overgrown with much smaller ones. Interestingly enough, EDS studies revealed no significant inhomogeneity in elemental distribution for all investigated specimens.

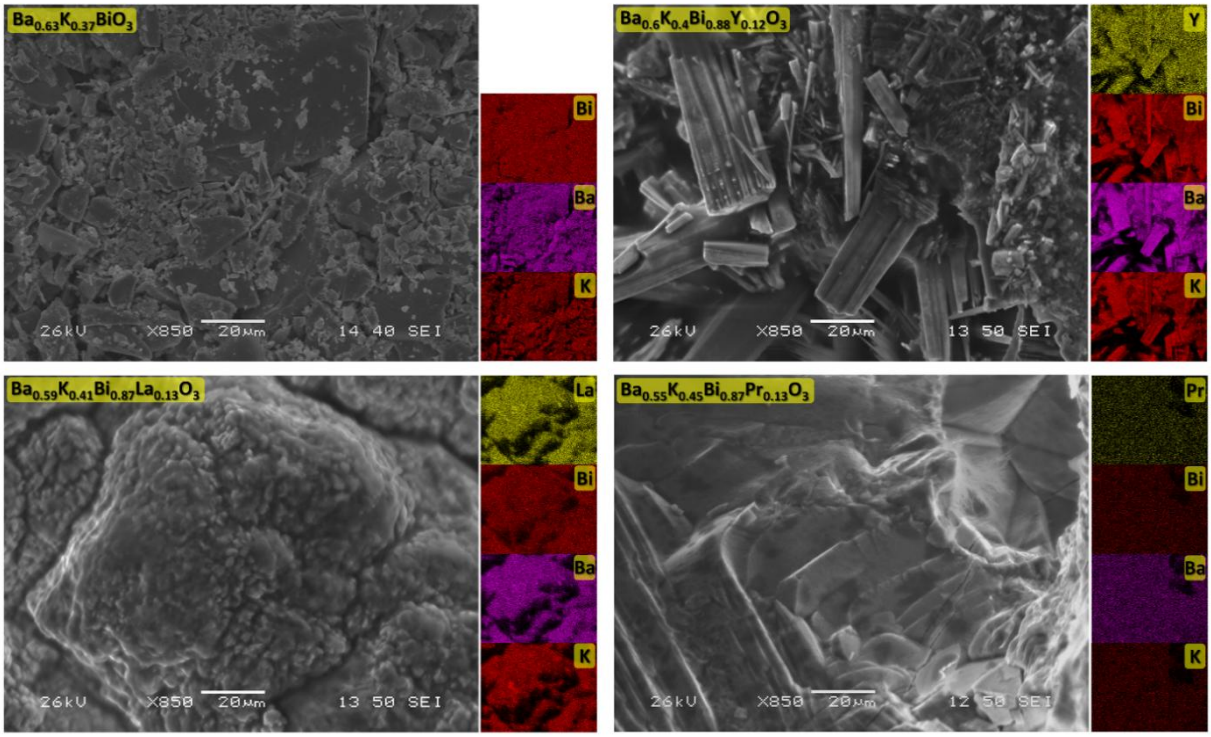

Figure 1. Microstructure of investigated compounds with X-ray microanalysis maps of elements' distribution.

In Table 1 the measured compositions by EDS were gathered. In general, the estimated values agree with the formal composition, however it can be noticed that a deficiency (2 ÷ 3 at%) of Y, La, Pr and Bi with similar excess of K and Ba elements occur.

Table 1. Results of X-ray microanalysis (EDS) for the investigated samples. Results are given in at%.

Sample	K-*K*	Ba-*L*	Bi-*L*	Y-*K*	La-*L*	Pr-*L*
$\mathbf{Ba_{0.63}K_{0.37}BiO_3}$	19.9(3)	32.5(3)	47.6(5)	-	-	-
$\mathbf{Y_{0.12}Ba_{0.6}K_{0.4}Bi_{0.88}O_3}$	22.0(3)	31.1(3)	41.1(4)	5.8(1)	-	-
$\mathbf{La_{0.13}Ba_{0.59}K_{0.41}Bi_{0.87}O_3}$	22.9(3)	29.1(3)	42.5(3)	-	5.5(1)	-
$\mathbf{Pr_{0.13}Ba_{0.55}K_{0.45}Bi_{0.87}O_3}$	22.2(2)	30.1(3)	41.9(3)	-	-	5.8(1)

3.2. Structural characterization

Collected X-ray diffraction (XRD) patterns revealed that the samples crystallize in the cubic $Pm\bar{3}m$ space group. Solely reflections originating from the $Ba_{0.63}K_{0.37}BiO_3$ and $RE_yBa_{1-x}K_xBi_{1-y}O_3$ (RE is Y, La or Pr) bismuth perovskites were observed confirming the excellent quality of the specimens. An example of refined XRD pattern for $Ba_{0.6}K_{0.4}Bi_{0.88}Y_{0.12}O_3$ is presented in Figure 2. For all investigated samples no traces of orthorhombic distortion ($I4/mcm$) were noticed. The Rietveld refinements provide lattice parameters for the investigated phases as gathered in Table 2. It was found that the constituents are distributed over the following positions: Ba and K at the *1a* site – 0, 0, 0; Bi and RE at the *1b* site – 0.5, 0.5, 0.5; O at the *3c* site – 0.5, 0.5, 0.

During refinements, the degree of occupancy of the 1*a* and *1b* sites by Ba/K and Bi/RE atoms were also the derived parameters as presented in Table 2. In our analyses, the hypothetical mixing of Ba/K/RE and Bi/K/RE was taken into account. However, the lowest reliability factors were obtained when Ba and K occupied solely the 1*a* site, while Bi and RE the 1*b* site.

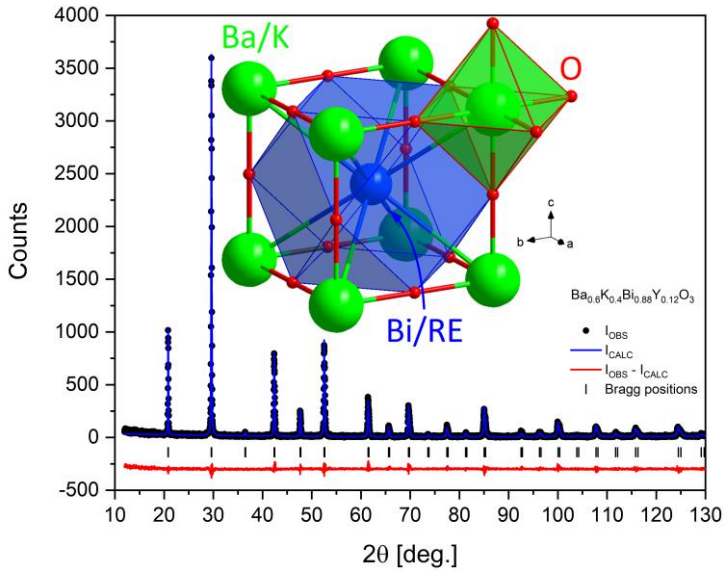

Figure 2. X-ray diffraction pattern of $Ba_{0.6}K_{0.4}Bi_{0.88}Y_{0.12}O_3$ with Rietveld refinement. Picture of the unit cell is given in the inset.

Table 2. Structural parameters for $RE_yBa_{1-x}K_xBi_{1-y}O_3$ at 300 K. Lattice parameter as well as stoichiometric indexes of K(x), RE(y), and reliability R_{Bragg} factors are given.

Sample	a [Å]	K(x)	RE(y)	R_{Bragg} [%]
$\mathbf{Ba_{0.63}K_{0.37}BiO_3}$	4.2875(2)	0.373(8)	-	5.6
$\mathbf{Y_{0.12}Ba_{0.6}K_{0.4}Bi_{0.88}O_3}$	4.2638(2)	0.406(8)	0.113(4)	5.4
$\mathbf{La_{0.13}Ba_{0.59}K_{0.41}Bi_{0.87}O_3}$	4.3046(2)	0.421(9)	0.122(5)	6.2
$\mathbf{Pr_{0.13}Ba_{0.55}K_{0.45}Bi_{0.87}O_3}$	4.2872(2)	0.458(9)	0.124(5)	6.1

As apparent from the structure of the unit cell (Figure 2), the Ba/K atoms in the center of octahedron of the O atoms (green polyhedron). The Ba/K–O bond length is about 2.14 Å. On the other hand, the Bi/RE position is enclosed within cuboctahedron formed by 12 O atoms (blue polyhedron). The Bi/RE–O bond length is about 3.03 Å, which is equal to the O–O one. In principle, the Ba/K–O bond is considered as the most important one, which is not necessarily true, as will be discussed later. It is worth mentioning that the calculated ab-initio lattice parameters presented in Section 2.2 behaves in the same way as experimental ones when different dopants (Y, La, Pr) were introduced.

As the BKBO's structure is extremely sensitive to stoichiometry, we performed XRD low-temperature studies to confirm that no structural changes at low temperatures occur. Indeed, in the 15 ÷ 300 K temperature range all reflections were solely described by the $Pm\bar{3}m$ cubic space group.

Based on the work of Marx et al. [49] and Braden et al. [50] a structural phase diagram for the $Ba_{1-x}K_xBiO_3$ system was proposed, according to which the highest value of x for which the perovskite structure was observed is approximately 0.5. Superconductivity is observed at x values from about 0.30 to 0.45. The maximum T_c reaches 34 K and occurs at x value of about 0.35. At room temperature, the crystal structure of the $Ba_{1-x}K_xBiO_3$

superconducting phases is regular, but as it was later established, their symmetry below the critical temperature of superconductivity is in fact tetragonal (*I*4/*mcm*) [50]. Moreover these phases are metastable and the transition from regular to tetragonal structure is continuous, while the transition from tetragonal to orthorhombic is discontinuous, and if the equilibrium temperature for tetragonal to orthorhombic transition is too low, it may simply not occur. In this case, superconductivity would occur only in the tetragonal metastable phase $Ba_{1-x}K_xBiO_3$, similar to the starting compound $BaPb_{1-x}Bi_xO_3$. Additionally, it was also shown that potassium deficient samples crystallize in orthorhombic *Ibmm* phase, while the excess of K in the material causes the precipitation of the secondary phase, $KBiO_2$ [51-53].

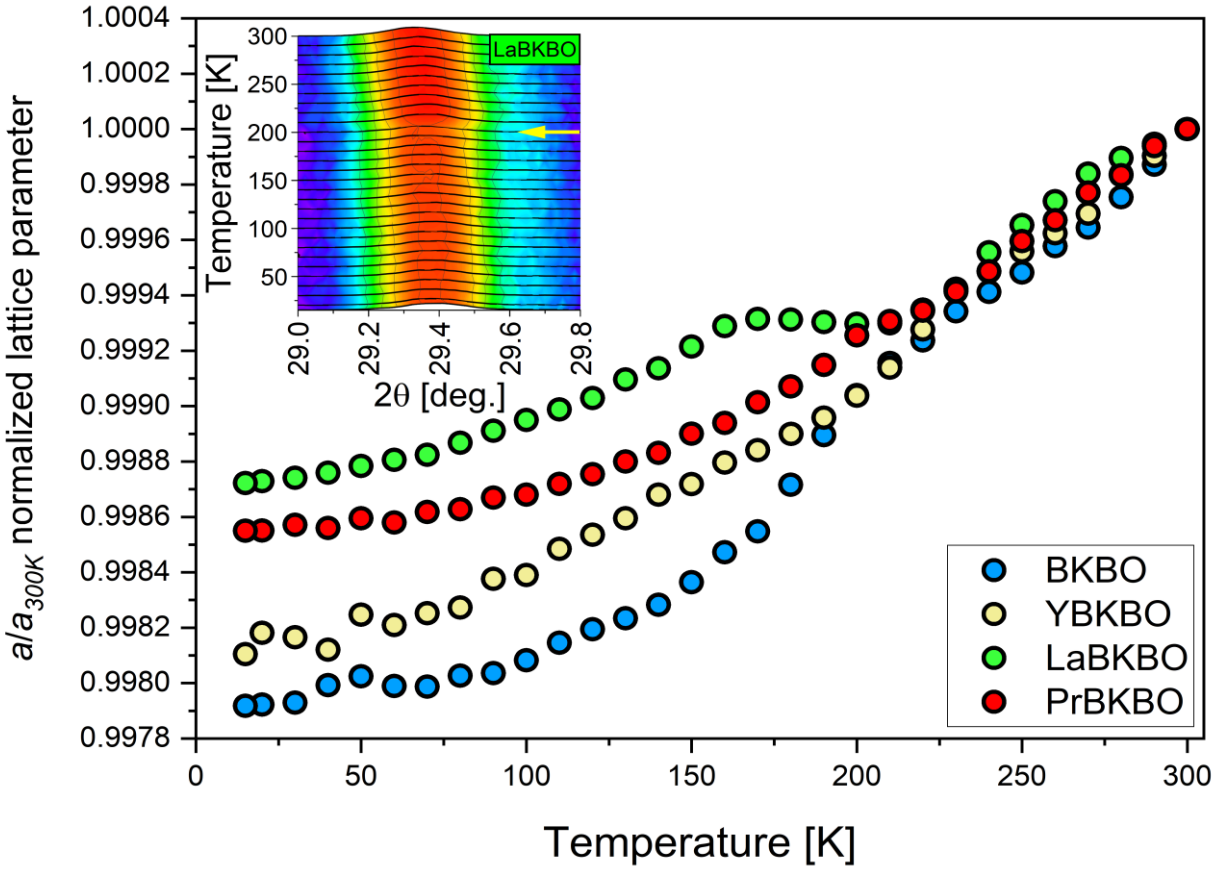

Figure 3. Low temperature X-ray diffraction studies of REBKBO compounds. The inset presents temperature dependence of the main 110 reflection for LaBKBO. Uncertainties are smaller than points' sizes.

In Figure 3 normalized lattice parameters versus temperature are gathered. Apparently, the behavior of BKBO and LaBKBO is anomalous at around 200 K. Namely, for BKBO the lattice shrink rapidly between 220 ÷ 160 K. On the other hand, completely different scenario is observed for LaBKBO, where lattice exhibits some kind of plateau between 220 ÷ 160 K. Additionally, at temperatures below 60 K some non-monotonous changes are visible for YBKBO and BKBO. For the latter sample those changes are probably related to superconducting transition that occurs at around 30 K.

Analysis of temperature dependence of the unit cell volume for cubic materials can be done using formula:

$$V \cong V_0 + I_C \frac{T^4}{\theta_D^3} \int_0^{\frac{\theta_D}{T}} \frac{x^3}{e^x - 1} dx \qquad \text{(Eq. 1)}$$

where: V_0 is the unit cell volume at 0 K, I_C is the coefficient including the Grüneisen and compressibility parameters and θ_D is the Debye temperature. The I_C coefficient can be considered as the slope of $V(T)$ dependence for temperatures above roughly 180 K. For investigated compounds those values are given in Table 3. Apparently, for BKBO and YBKBO the refined parameters can be biased by anomalous thermal expansion.

Table 3. Parameters of the Eq. (1) as derived for REBKBO samples: V_0 is the extrapolated unit cell volume at 0 K, I_C is the coefficient including the Grüneisen and compressibility parameters and θ_D is the Debye temperature.

Sample	θ_D [K]	V_0 [Å^3]	I_C [Å^3/K]
$Ba_{0.63}K_{0.37}BiO_3$	450(35)*	78.33(2)*	0.00612(4)*
$Ba_{0.6}K_{0.4}Bi_{0.88}Y_{0.12}O_3$	355(15)	77.08(1)	0.00676(2)
$Ba_{0.59}K_{0.41}Bi_{0.87}La_{0.13}O_3$	245(31)*	79.46(2)*	0.00428(4)*
$Ba_{0.55}K_{0.45}Bi_{0.87}Pr_{0.13}O_3$	490(12)	78.46(1)	0.00662(2)

* Derived from 15 – 160 K temperature range.

For YBKBO and PrBKBO the parameters were derived from the full temperature range, while for BKBO and LaBKBO from region below 160 K, only. However, comparison of the Debye temperatures for YBKBO and PrBKBO show significant differences, yielding quite distinct phononic properties of the compounds.

3.3. Magnetic characterization

Magnetic characterization of REBKBO compounds by means of DC magnetization is presented in Figure 4. Magnetization studies were performed at fields of 20 Oe and 100 Oe for BKBO, and at fields of 10 Oe and 20 Oe for other compositions (only 20 Oe curves are presented).

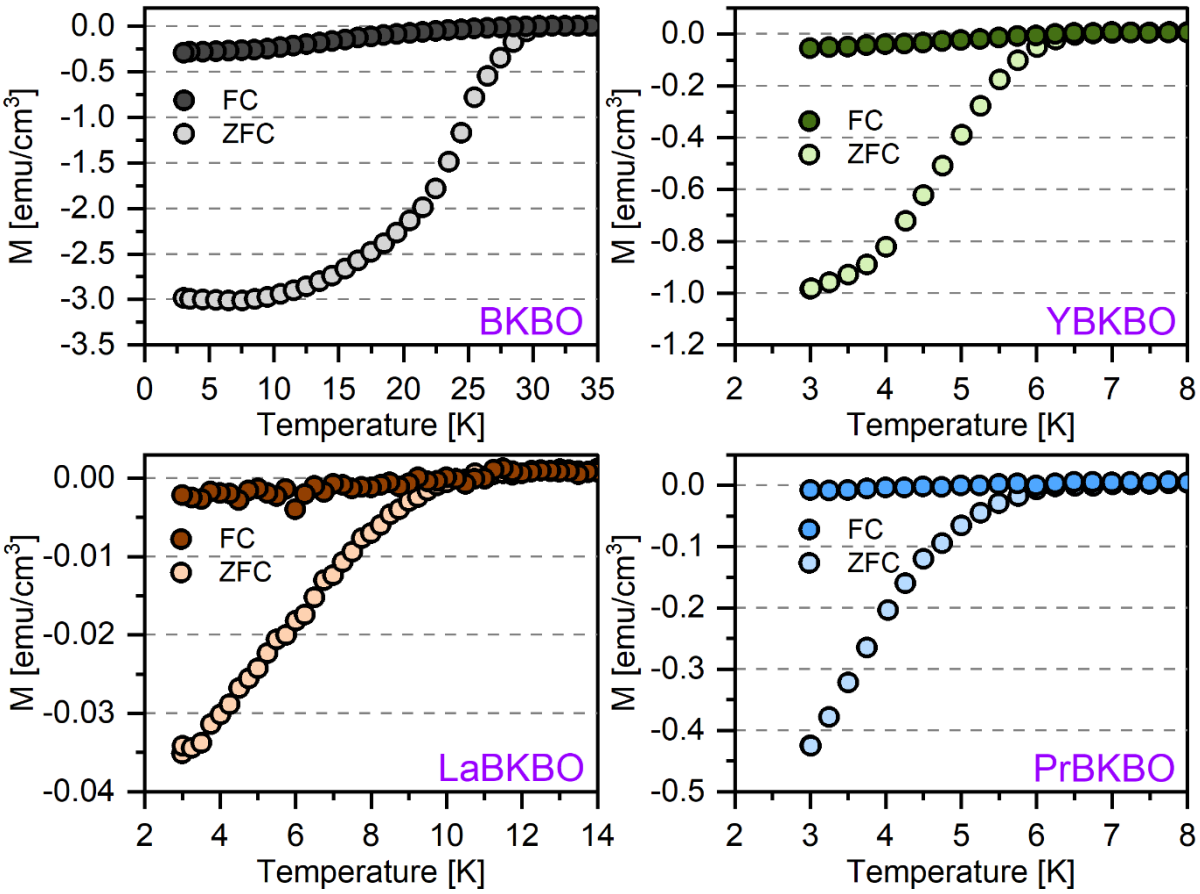

Figure 4. Temperature dependence of volume magnetization $M(T)$ at field of 20 Oe for the investigated samples. ZFC – zero field cooling, FC – field cooling.

For all samples ZFC and FC curves undergo splitting at temperatures of 30.1 K (BKBO), 6.5 K (YBKBO), 11.3 K (LaBKBO) and 6.3 K (PrBKBO), which may be associated to onset of the superconducting state. As apparent from the Figure 4, the lowest magnetization was observed for LaBKBO, which is an order of magnitude lower than that for PrBKBO or YBKBO and two orders of magnitude lower than for BKBO. The PrBKBO does not exhibit long-range magnetic ordering despite having the $4f^2$ electronic configuration. Presumably due to the singlet of the splitted ground multiplet as a consequence of Crystalline Electric Field (CEF).

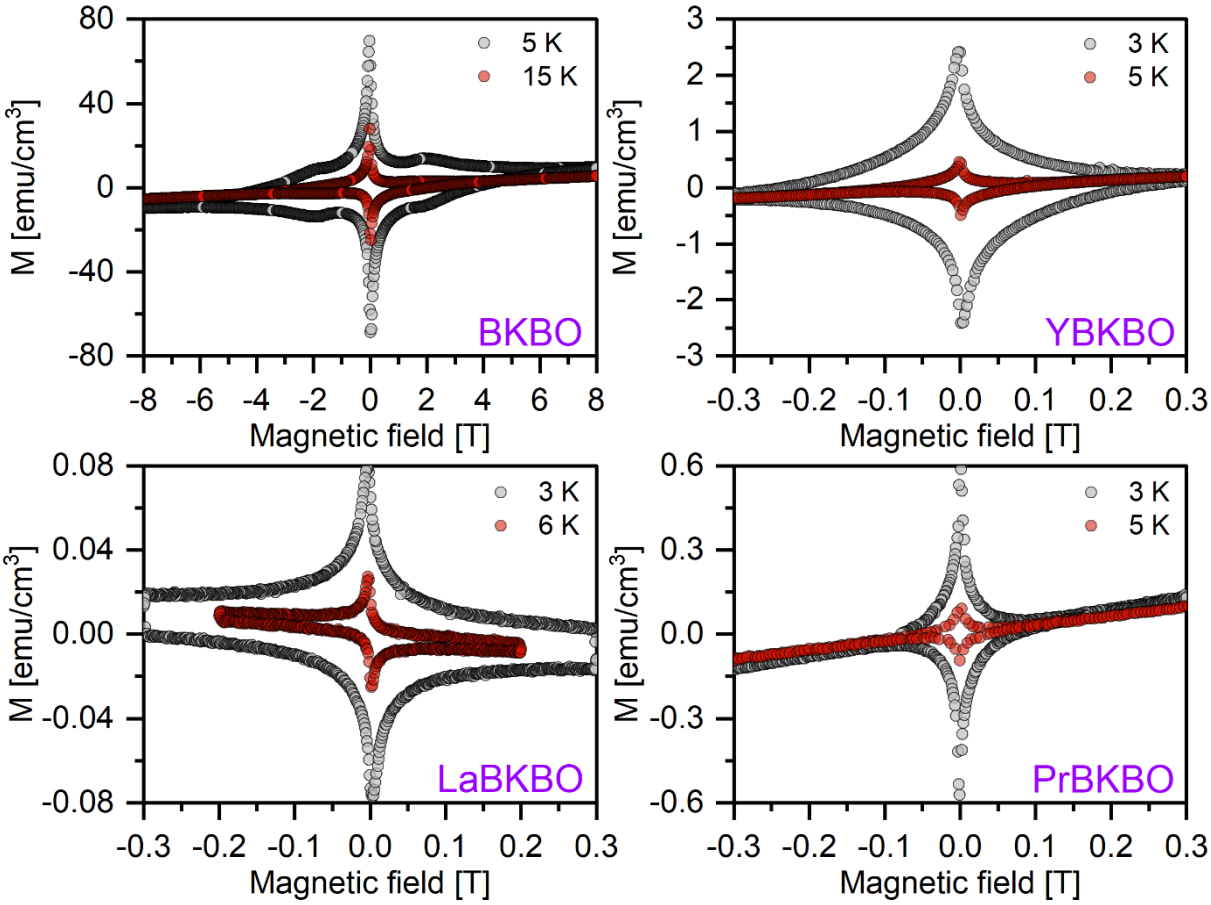

Figure 5. Isothermal magnetization as a function of magnetic field for REBKBO samples. Only chosen curves below critical temperature are presented in sake of pictures' clarity.

Inspection of hysteresis loops recorded for REBKBO samples brings very intriguing results, which are shown in Figure 5. Namely, for all samples except the LaBKBO the superconducting signal is overlayed on the paramagnetic one, as the background line shows positive d*M*/d*T* derivative. The LaBKBO shows completely different behavior with diamagnetic background. For BKBO an additional maximum at field of about 2.5 T is evidenced, which appearance is called the Second Peak Effect (SPE). The SPE originates from arising additional pinning centers at higher fields, likely due to randomly located oxygen/potassium non-stoichiometry. Interestingly enough, such effect was not observed in other compositions.

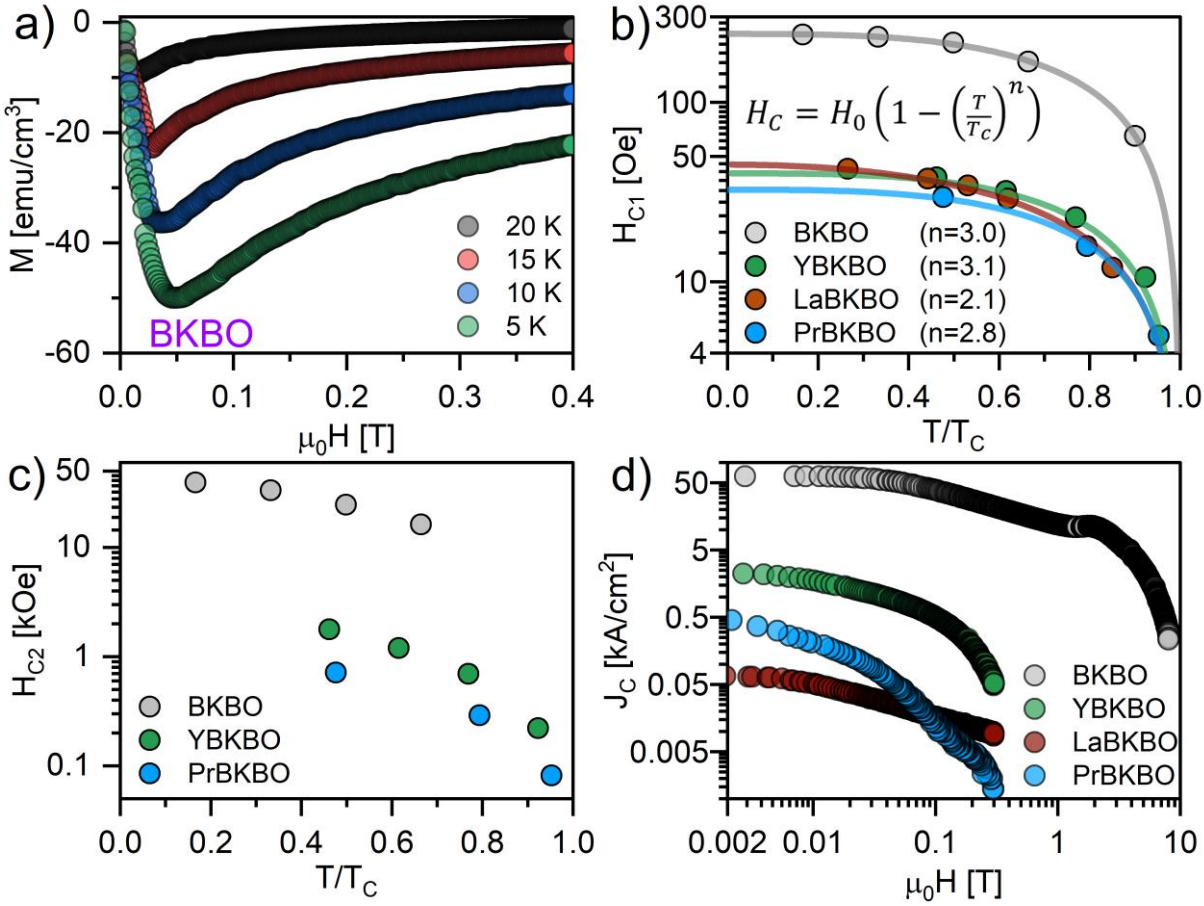

Figure 6. Various superconducting characteristics for REBKBO: (a) examples of virgin magnetization curves for BKBO; (b) and (c) 1st (H_{c1}) and 2nd (H_{c2}) critical fields; d) critical current density (J_c) versus magnetic field (M) at the lowest measured temperature. Solid lines in the part (b) show the scaling of H_{c1} according to the given formula.

In Figure 6a, an example of virgin magnetization curves for BKBO are presented. From those curves, measured for all compounds, first critical field H_{c1} was estimated as deviation from linear behavior of $M(H)$ for small fields (Figure 6b). In addition the second critical field H_{c2} was plotted in the Figure 6c. For LaBKBO the estimation of H_{c2} would require extraction of diamagnetic background, however this procedure introduced large uncertainty of so-derived critical field therefore we decided to skip that analysis. The H_{c1} obey the typical scaling with the temperature: $H_c = H_0\left(1-\left(\frac{T}{T_c}\right)^n\right)$, which was plotted as

solid lines in Figure 6b. Interestingly, the critical exponent for BKBO, YBKBO and PrBKBO is close to 3, while for LaBKBO its value very different and equal 2.1. The latter value corresponds well to typical BCS scaling of the thermodynamical critical field. Yet, very different behavior of the other compositions must be underlined.

By using the Bean critical-state model one can estimate the superconducting critical current density (J_c) of REBKBO according to the formula:

$$J_c(H) = \frac{20 \cdot \Delta M(H)}{a \cdot (1 - \frac{a}{3b})}, \qquad \text{(Eq. 2)}$$

where *a* and *b* are the sample dimensions perpendicular to the applied magnetic field, and *M* is a difference in $M_{\downarrow} - M_{\uparrow}$ volume magnetizations when sweeping field in opposite directions. The calculated critical currents are presented in the Figure 6d. It is clearly visible that critical current density for BKBO surpasses values obtained for YBKBO by one order of magnitude, for LaBKBO by two and finally for PrBKBO by three orders of magnitude. However, once again an anomalous behavior was evidenced for LaBKBO sample. For that specimen magnetic field suppresses J_c significantly lower than for PrBKBO leading to crossing both curves at 0.085 T.

3.4. Specific heat measurements

Heat capacity studies for the investigated samples revealed that no distinct anomalies related to superconducting transitions were observed (Figures 7 and 8). Moreover, applied magnetic field of 8 T did not alternate the heat capacity significantly except for PrBKBO, which will be discussed later.

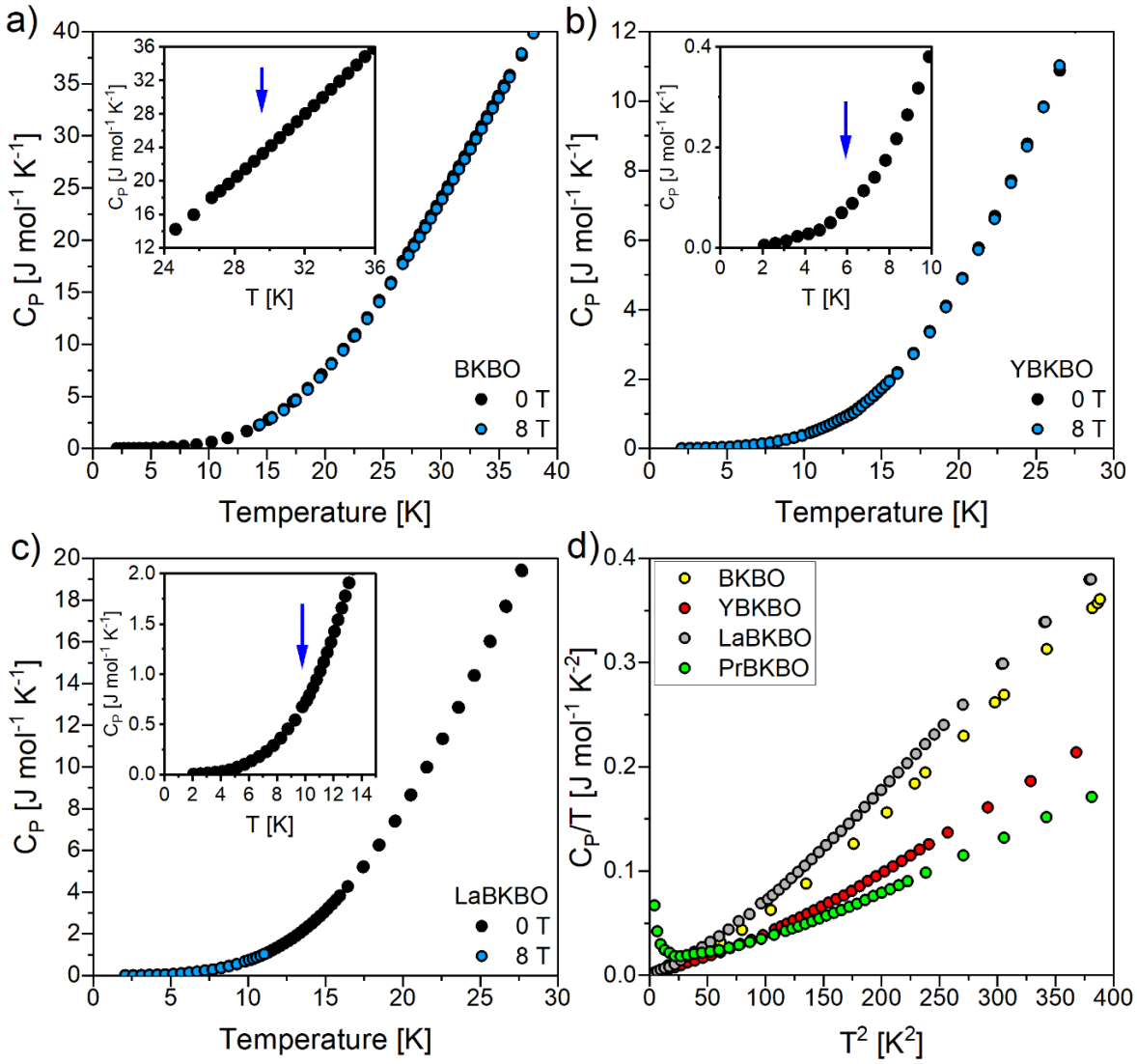

Figure 7. Heat capacity studies for REBKBO.

In the low temperature region (below the critical temperature) the temperature dependence of specific heat can be approximated by:

$$C_{\mathrm{P}} = 9nR\frac{4\pi^4}{5}\left(\frac{T}{\theta_{\mathrm{D}}}\right)^3 + C_0 e^{-\frac{\Delta}{k_{\mathrm{B}}T}} \qquad \text{(Eq. 3)}$$

where θ_D is the Debye temperature, R – gas constant, n – number of atoms per f.u. and Δ the superconducting gap. We did not included the Sommerfeld specific heat as formation of the superconducting state opens gap at the Fermi level, therefore contribution of the conducting electrons to the γ coefficient can be assumed to be negligible small. For investigated compounds the Equation (3) gives values of Debye temperature comparable to XRD studies except the value for BKBO, which is much lower (θ_D are given in Table 4). However, one must keep in mind that in XRD data anomalous behavior was evidenced for that sample. The values for PrBKBO were biased by upturn of C_p at low temperatures (see the Figure 8) therefore only first term of the Equation (3) were taken into account above the critical temperature (including the Sommerfeld coefficient). Low-temperature specific heat in general obeys the activation behavior with superconducting gap. The dimensionless R_Δ ratio is close to BCS weak/medium coupling regime (Table 4), as for the similar BKBO compound [54].

Table 4. Parameters of the Eq. (3) as derived for REBKBO samples θ_D is the Debye temperature, Δ is the superconducting gap, $\frac{2\Delta}{k_B T_c}$ is dimensionless ratio (R_Δ) of BCS theory.

Sample	θ_D [K]	Δ [meV]	$\frac{2\Delta}{k_B T_c}$
$Ba_{0.63}K_{0.37}BiO_3$	248(6)	4.27(5)	3.29
$Y_{0.12}Ba_{0.6}K_{0.4}Bi_{0.88}O_3$	321(8)	1.05(3)	3.75
$La_{0.13}Ba_{0.59}K_{0.41}Bi_{0.87}O_3$	239(4)	1.81(5)	3.69
$Pr_{0.13}Ba_{0.55}K_{0.45}Bi_{0.87}O_3$	420(8)	-	-

According to our calculations, presented in Section 4, the low values of Sommerfeld coefficient around 1 mJ/mole·K^2 can be used for estimation of specific heat jump at the transition into superconducting state. Namely, for BKBO the jump will be less than 45

mJ/mole·K^2, while for other samples less than 10 mJ/mole·K^2. Therefore, it is not surprising that no distinct anomalies were detected.

The upturn of C_P at low temperatures for PrBKBO can be understood in terms of Schottky contribution related to CEF splitting of the ground Pr^{3+} multiplet. Applying the magnetic field leads to higher splitting of the Schottky levels, hence further raise of the low-temperature specific heat. In such a case Magneto-Caloric Effect (MCE) was expected.

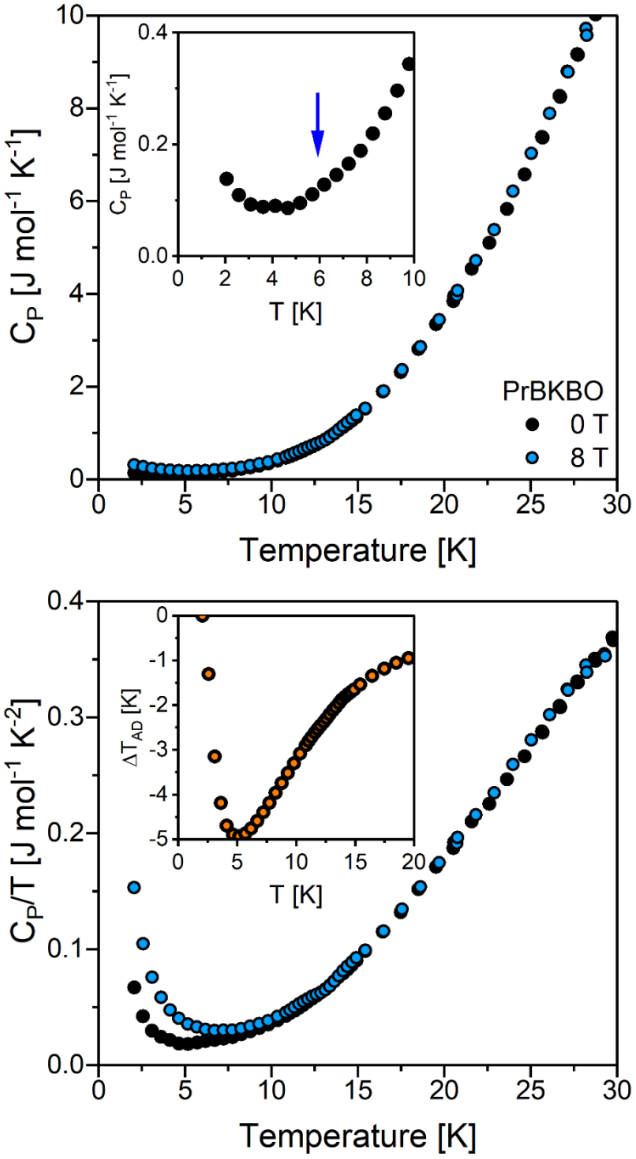

Figure 8. Heat capacity studies and magnetocaloric effect for PrBKBO.

After calculating entropy change due to magnetic field presence, the adiabatic temperature change ΔT_{AD} was estimated (see inset to the Figure 8). The adiabatic temperature change exhibits the highest value at around 5 K, which is just around the critical temperature for that compound. It is worth noting that this sample exhibits negative MCE. In principle, MCE (positive) is currently widely studied and discussed in manganites, eg. $LaMnO_3$ [55], while for BKBO-related specimens was not found yet, to our best knowledge.

3.5. FT-IR (Fourier-Transform Infrared Spectroscopy) measurements

In Figure 9 IR spectra recorded for samples at 298 K and 13 K are gathered. The observed peaks positions and their proposed assignments are summarized in Table 5.

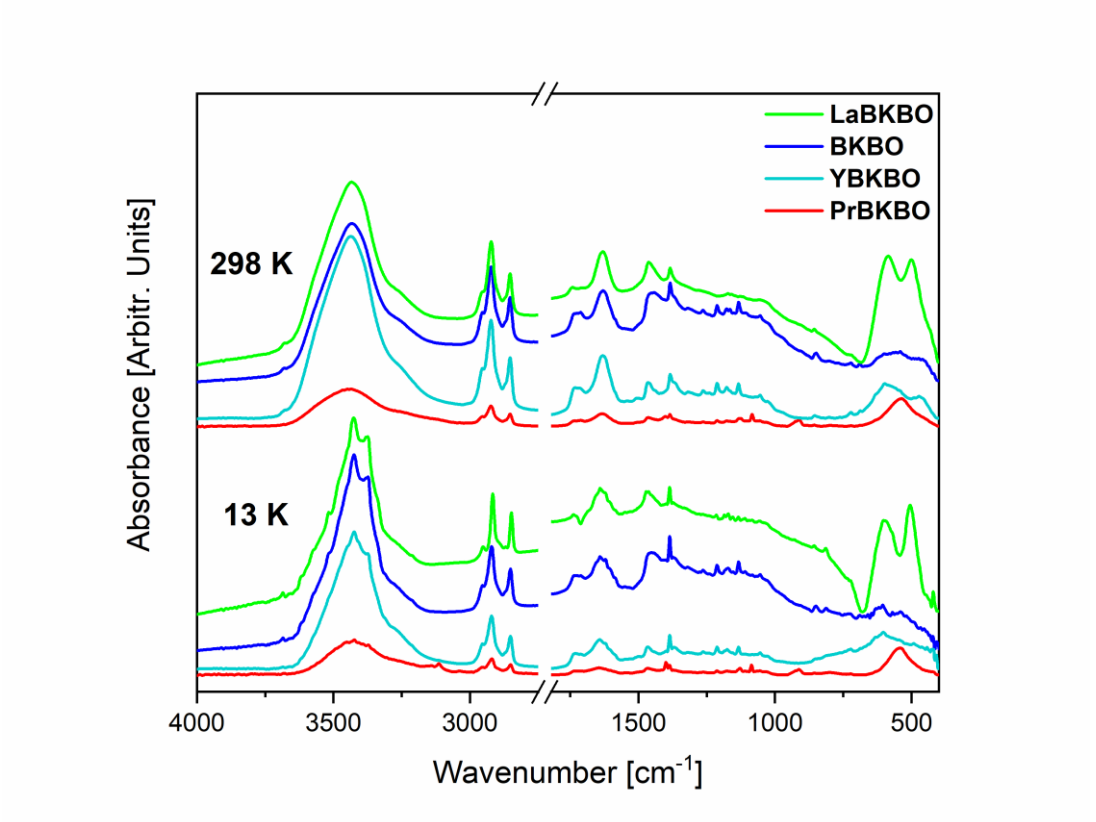

Figure 9. FT-IR spectra of REBKO recorded at 298 K and 13 K in the wavenumber range of 4000 ÷ 400 cm^{-1}.

Table 5. Observed wavenumbers (cm^{-1}) and assignments for the studied samples [56,57].

Assigments	BKBO		YBKBO		LaBKBO		PrBKBO	
	298 K	13 K	298 K	13 K	298 K	13 K	298 K	13 K
δ(Bi–O–Bi)	462 sh		469 sh		500 vs	503 vs		
ν(Bi–O)	518 m	539 br 605 br	602 br	602 br	583 vs	591 vs	533 vs	540 vs
ν(Bi–O)	693 w							
δ(Bi–O–Bi)							797 br	795 br
δ(Bi–O–Bi)		813 w				814 w		
ν(Bi–O)	848w 855w	849 w 855 w	852 w	853 w	856 w	856 w	856 w	856 w
ν(Bi–O) in distorted BiO_{12}							911 s	912 s
ν(Bi–O) in distorted BiO_{12}							924 sh	924 sh
ν (C–O)							1084 s 1125 m	1086 s 1127 m
ν(Bi–O)	1384 s	1386 s	1384 s	1386 s	1384 s	1386 s	1384 s	1386 s
ν(O–H)							1401 m	1399 s
β(Ba–O) bending vibrations	1439 s	1454 s	1464 m	1463 m	1463 s	1462 s 1474 s	1463 m	1463 m
(H–O) bending vibrations of water	1563 sh	1547 br						
β(H–O) bending vibrations of water	1631 s	1620 s 1640 s	1631 s	1620 sh 1641 s	1629 s	1640 s	1644 s	1644 s
C=O	1738 sh 2170 w	1738 br 2172 wv	1731 br	1732br	1741 br	1737 br	1711 br 2170 w	1709 br 2170 vw
	2853 s 2921 s 2957 sh	2851 s 2920 s 2953 sh	2852 s 2922 s 2954 sh	2851 s 2920 s 2954 sh	2853 s 2922 s 2954 sh	2848 s 2916 s 2952 sh	2852 s 2923 s 2954 sh	2850 s 2918 s 2956 sh
v(O–H)	3435 vs	3371 sh 3424 vs	3434 vs	3371 sh 3424 vs	3432 vs	3372 vs 3425 vs 3684 w	3439 vs	3113 s 3422 vs

(vw - very wek, aw - weak, br - broad, sh - shoulder, m - medium, s - strong, vs - very strong, ν - stretching, δ - bending-in-plane).

The spectral image of the BKBO, LaBKBO and YBKBO samples indicates the presence of two active bands in the range of 400 ÷ 700 cm^{-1}. These bands are attributed to the stretching vibrations of Bi single bond O and Bi–O–Bi in [BiO_{12}] structural units [56,57]. Doping of sample leads to shifting of the at 462 and 518 cm^{-1} bands and changing in their relative intensity. It results from the substitution of heavier and less electronegative La^{3+} and Y^{3+} ions in the place of Bi^{3+}. The greatest difference in the spectrum compared to the undoped sample was recorded for PrBKBO. In the spectrum of this sample in the range of 400 ÷ 700

cm^{-1} only one single band at 500 cm^{-1} is visible. What is more, the spectrum of this sample revealed the existence of the bands near 800 and 900 cm^{-1} connected with stretching vibrations of Bi–O bonds in strongly distorted BiO_{12} units. Additionally, H_2O, CO_2 and likely bicarbonate compounds adsorbed on the surfaces and pores are visible as different O–H and C=O bands.

Cooling the samples down to 13 K has the strongest effect on the band occurring around 500 cm^{-1} attributed to the stretching vibrations of Bi–O in BiO_{12} unit. The shift of the position of this peak towards the higher wavenumber proves that the frequency of Bi–O vibrations described by this band increases at the low temperature. Moreover, cooling BKBO and PrBKBO samples leads to the appearance of a new band at ca. 813 cm^{-1}. This band was attributed to the bending vibration of Bi–O–Bi.

To check whether the changes occurring during cooling each of the samples can be additionally visualized by examining the temperature evolution of the mid-infrared spectra, the statistical cluster analysis of spectra was performed using OPUS software package. Cluster analysis takes into account all the variability in the data and shows the similarity or dissimilarity between each pair of spectra collected for a given sample at different temperatures. The goal of the grouping algorithm is to divide the objects into homogeneous groups so that the intragroup similarities are large compared to the similarities between the groups.

The cluster analysis results supported the results of magnetic and structural study conducted for BKBO and PrBKBO samples (Figure 10). The dendrogram shown in Figure 10a indicates that is possible to observe three distinct spectral groups (green, pink and red branches of the dendrogram) differentiating in the vicinity of 193 and 73 K. These temperatures correspond to structural and magnetic transitions observed in BKBO sample.

In turn the dendrogram obtained for PrBKBO sample (Figure 10b) indicates the presence of three distinct spectral groups, but differentiating in the vicinity of 193 and 33 K. These temperatures also correspond well with structural and magnetic transitions observed in PrBKBO sample.

The cluster analysis perform for LaBKBO and YBKBO samples did not give an unequivocal result. It was not possible to group the temperature dependent spectra into homogeneous groups with a high degree of similarity. Obtained results suggest that phase transitions observed for LaBKBO and YBKBO compounds are not visible from an infrared spectroscopy point of view.

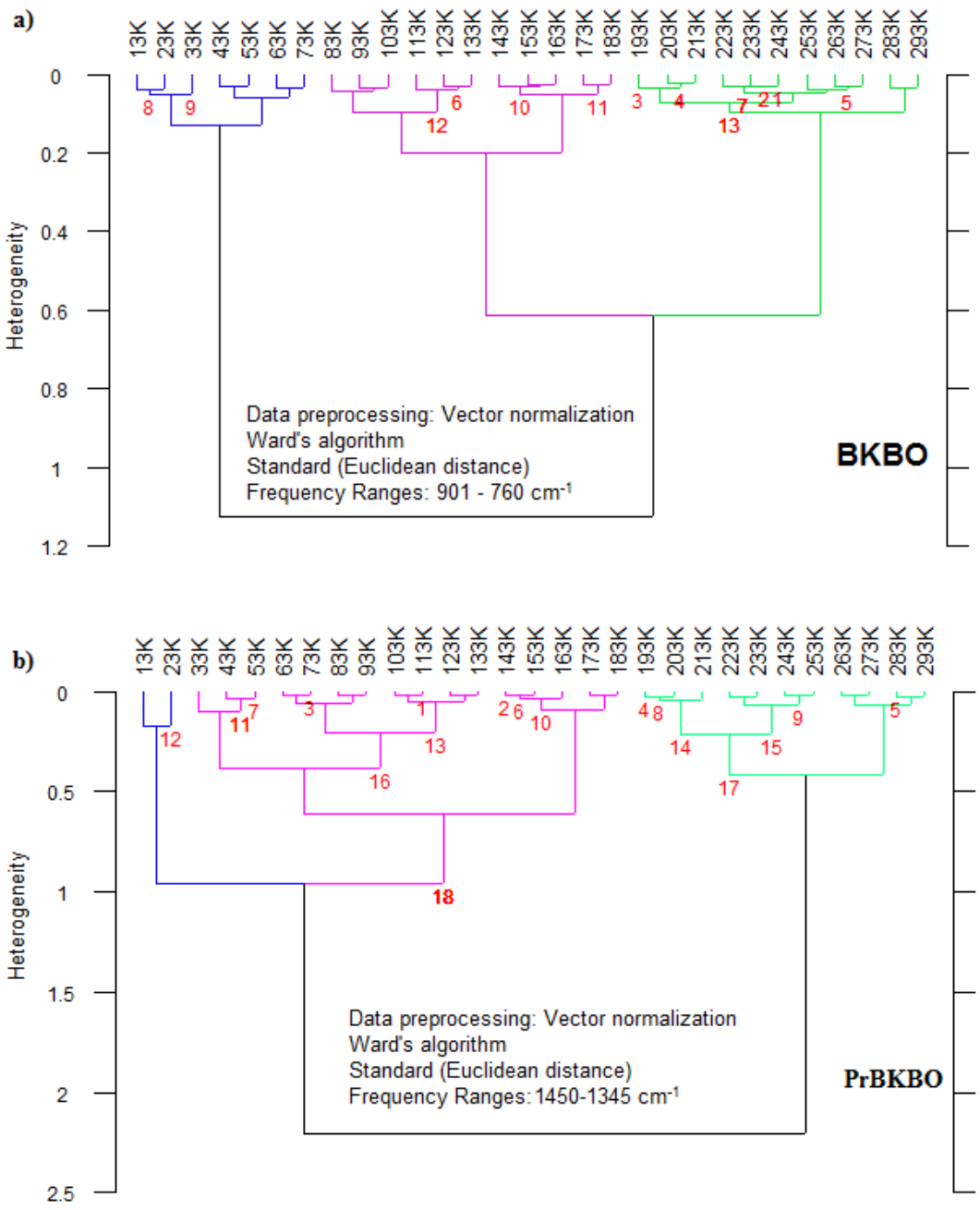

Figure 10. Dendrogram of a Hierarchical Cluster Analysis performed on FT-IR spectra of (a) BKBO and (b) PrBKBO samples

4. Ab-initio electronic structure studies

Electronic structure calculations revealed that the investigated compounds exhibit some crucial differences in the DOS near the Fermi level, as depicted in Figures 11 and 12. The contribution to the DOS at the E_F originates mainly from the O-2*p* and the Bi-6*s* and 6*p*

states. The Ba-5*d* states are about 2 eV below E_F and presumably do not play a major role. Similarly, Y and La exhibit negligible contribution to the DOS(E_F). Even though they do not contribute directly, they influence strongly the O-2*p* states due to hybridization. Similar situation holds for the K states. Finally, the Pr acts as electron dopant to the E_F (the 4*f* states) and has significant impact on the O-2*p* and the Bi-6*s* states, at the same time.

A closer inspection of the Bi contribution to the E_F suggests that its contribution is highest for BKBO (a distinct peak at E_F), while for Y and La-based systems the peak is smaller. For those systems a gap is visible around 0.5 eV below the E_F, which is absent for the Pr-based specimen. Additionally, the peak observed for BKBO, YBKBO and LaBKBO at E_F is diminished for PrBKBO.

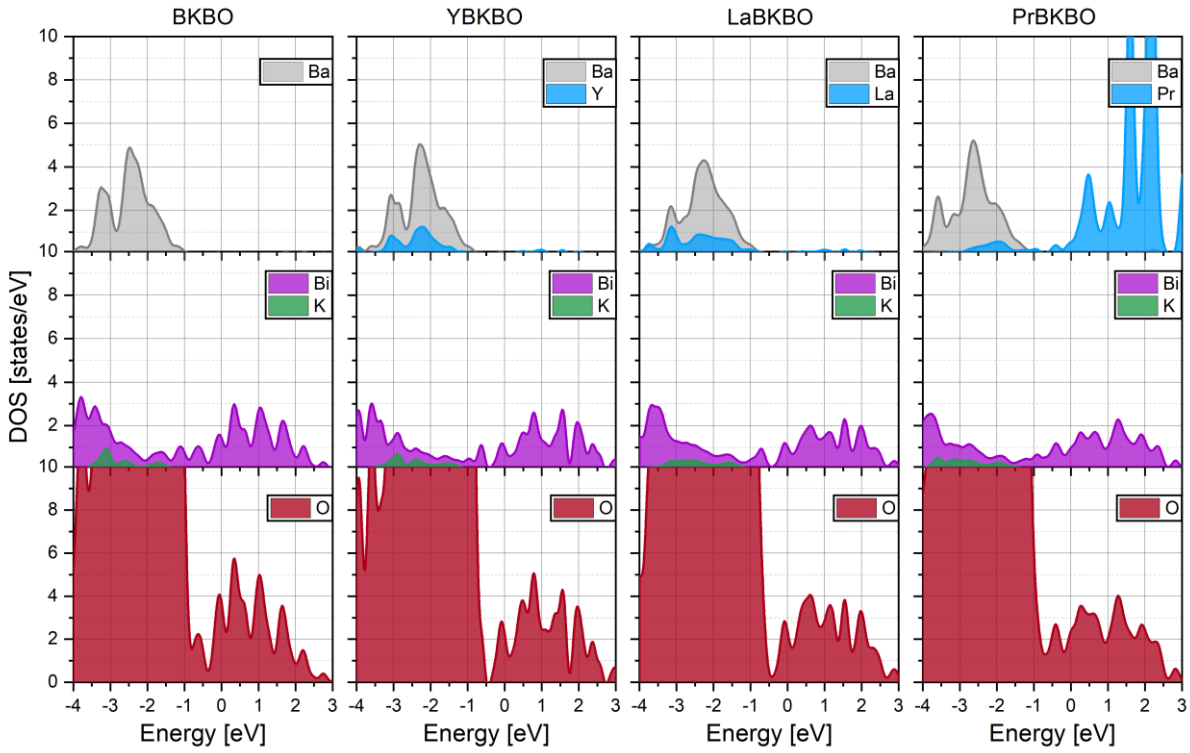

Figure 11. Partial density of states per 2x2x2 supercell for the investigated REBKBO compounds. Energy 0 eV refers to the Fermi energy (E_F) level.

Similar observations can be made for the O-2*p* states. For all systems, except the PrBKBO, there is well-defined peak at the E_F and a gap 0.5 eV below the Fermi level. However, the amplitude of the peak is suppressed by introducing the dopants by about 25%. For the PrBKBO, situation is significantly changed. The gap in the O-2*p* states closes and the peak shifts below the E_F. Consequently, the partial oxygen DOS(E_F) is the smallest. For the latter system, the empty 4*f* states appear between 1.5 ÷ 2.5 eV above the E_F.

Table 6. Calculated values of density of states at the Fermi level (for the unit cell) and the Sommerfeld coefficient γ.

Sample	DOS [states/eV]	γ [mJ/mole·K^2]
$\mathbf{Ba_{0.63}K_{0.37}BiO_3}$	0.674	1.583
$\mathbf{Y_{0.12}Ba_{0.6}K_{0.4}Bi_{0.88}O_3}$	0.414	0.973
$\mathbf{La_{0.13}Ba_{0.59}K_{0.41}Bi_{0.87}O_3}$	0.446	1.048
$\mathbf{Pr_{0.13}Ba_{0.55}K_{0.45}Bi_{0.87}O_3}$	0.498	1.171

As apparent from the Figure 12 and Table 6, the parent BKBO compound shows the highest DOS(E_F), in comparison to doped systems. One would expect that this system exhibits the highest critical temperature. Indeed, this trend is visible for all systems except the Pr-BKBO, which has slightly higher DOS(E_F), but the lowest critical temperature. Presumably, the magnetic properties of the Pr^{3+} hamper the superconducting interactions despite presumably singlet state of the CEF multiplet.

The calculated Sommerfeld coefficients of electronic specific heat are similar to those reported for $Ba_{1-x}K_xBiO_{3-y}$ system based on wide temperature range specific heat data [58].

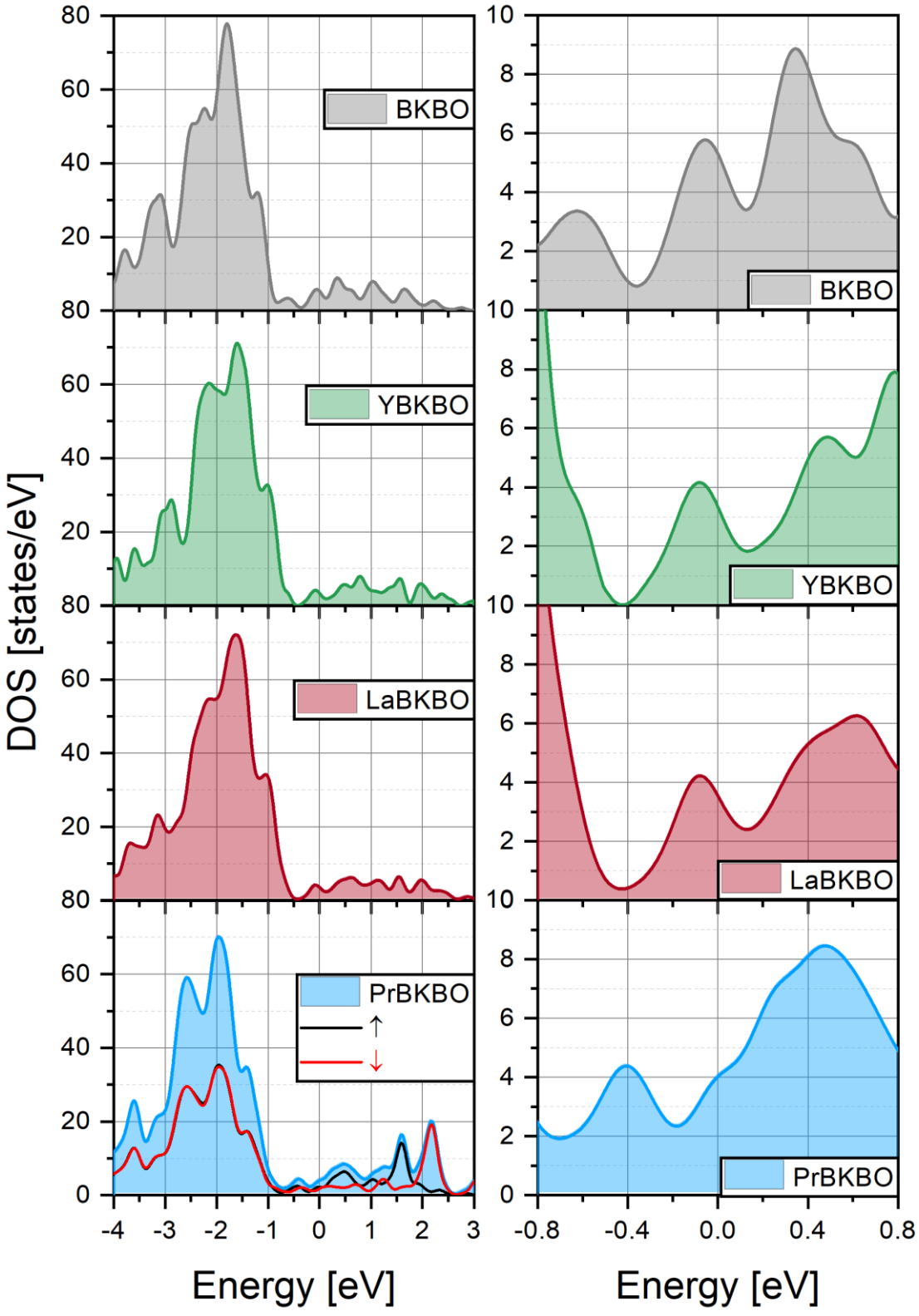

Figure 12. Total density of states per 2x2x2 supercell for the investigated REBKBO compounds. Energy 0 eV refers to the Fermi energy (E_F) level.

5. Concluding remarks

Low-temperature structural studies revealed significant differences and anomalies in thermal expansion and lattice dynamics. Apparently, small doping of different elements into Bi leads to significant changes of phononic properties as evidenced from XRD and FT-IR data. The cluster analysis of FT-IR data for BKBO and PrBKBO reveals that at temperatures below 200 K some reorganization of observed bonds excitations happens. This is in agreement with peculiar behavior of the lattice parameter as derived from XRD. Additional, region below 73 K for BKBO is presumably related to gradual changes of phononic structure to get ready to transition into HTS state. On the other hand, for PrBKBO cluster analysis shows additional changes of lattice dynamics below 33 K, which is likely related to gradual depopulation of higher levels of the CEF Pr^{3+} multiplet. The latter is in agreement with negative magnetocaloric effect and specific heat studies. The highlight of the structural properties is that the lattice expansion is anomalous in both BKBO and PrBKBO, however the nature of the behavior seems opposite.

Suppression of superconductivity for doped BKBO system is reflected by dumping of critical temperatures and current densities that are: 30.1 K and 65 kA/cm^2 (BKBO); 6.5 K and 2.3 kA/cm^2 (YBKBO); 6.3 K and 0.46 kA/cm^2 (PrBKBO); 11.3 and 0.07 kA/cm^2 (LaBKBO). As evidenced, the doped samples exhibit different critical scaling exponents for first critical magnetic field (H_{c1}). The critical exponents for BKBO, YBKBO and PrBKBO are close to 3, while for LaBKBO is close to 2. The distinct temperature and field responses of superconducting parameters for LaBKBO correlate clearly to anomalous lattice dynamics evidenced by XRD. It seems that the electronic structure itself is not the key reason for the abovementioned anomalous behavior while for BKBO, YBKBO and LaBKBO electronic structure in the vicinity of the Fermi level seems similar.

Electronic structure calculations revealed that despite almost the same distances between Ba/K–O and Bi/RE–O that were detected for BKBO and PrBKBO the DOS(E_F) is substantially modified. This conclusion reflects importance of the 4*f* element doping into the Bi position, as it depletes O-2*p* states. Therefore, it would be desirable to extent the future research on BKBO doped by other 4*f* /5*f* elements.

Acknowledgements

This work was accomplished in close collaboration with the group of prof. Neven Barišić from the Institute of Solid State Physics of TU Wien, Austria. The study was partially financed by foreign cooperation between the Faculty of Mathematics and Natural Sciences of Cardinal Stefan Wyszyński University (CSWU) in Poland and TU Wien (TUW) in Austria. The authors would like to thank prof. Neven Barišić from TUW in Austria and prof. Wojciech Tabiś from TUW in Austria and AGH University of Science and Technology in Poland for their kindness and valuable discussions on the measurements carried out.

Naveen Kumar Chogondahalli Muniraju acknowledges support from the Polish National Agency for Academic Exchange under the 'Polish Returns 2019' program, grant PPN/PPO/2019/1/00014.

Anna Krztoń-Maziopa acknowledges the partial support provided by statutory budget of Faculty of Chemistry, Warsaw University of Technology in Poland.

Competing interests

The authors declare that they have no personal relationships or financial dependencies with any organization or with anyone who would have a direct financial contribution to the subject of research or materials studied in this work.

CRediT authorship contribution statement:

Paweł Peczkowski: Conceptualization, Methodology, Validation, Formal analysis, Investigation, Writing – original draft, Writing – review & editing, Visualization, Data curation, Supervision, Project administration, Funding acquisition. **Maciej Łuszczek:** Writing – review & editing, Data curation, Software. **Elżbieta Szostak:** Investigation, Writing – original draft, Writing – review & editing. **Naveen Kumar Chogondahalli Muniraju:** Investigation, Funding acquisition. **Anna Krztoń-Maziopa:** Resources, Writing – review & editing, Funding acquisition. **Łukasz Gondek:** Formal analysis, Investigation, Writing – original draft, Writing – review & editing, Visualization, Data curation, Supervision.

References

[1] A. Glatz, I.A. Sadovskyy, U. Welp, W.-K. Kwok, G.W. Crabtree, The quest for high critical current in applied high-temperature superconductors, J. Superconduc. Nov. Mag. 33 (2020) 127–141.

[2] W.D. Markiewicz, D.C. Larbalestier, H.W. Weijers, A.J. Voran, KW. Pickard, W.R. Sheppard, J. Jaroszynski, A. Xu, R.P. Walsh, J. Lu, A.V. Gavrilin, P.D. Noyes, Design of a superconducting 32 T magnet with REBCO high field coils, IEEE Trans. App. Superconduc. 22(3) (2012) 4300704.

[3] H.K. Onnes, The resistance of pure mercury at helium temperature, Commun. Lab. Phys. Univ. Leiden 12 (1911) 120.

[4] L. Gao, Y.Y. Xue, F. Chen, Q. Xiong, R.L. Meng, D. Ramirez, C.W. Chu, J.H. Eggert, H.K. Mao, Superconductivity up to 164 K in $HgBa_2Ca_{m-l}Cu_m0_{2m+2+6}$ (m = l, 2, and 3) under quasihydrostatic pressures. Phys. Rev. B 50 (1994) 4260–4263.

[5] A.P. Drozdov, M.I. Eremets, I.A. Troyan, V. Ksenofontov, S.I. Shylin, Conventional superconductivity at 203 kelvin at high pressures in the sulfur hydride system, Nature 525 (2015) 73–76.

[6] E. Snider, N. Dasenbrock-Gammon, R. McBride, M. Debessai, H. Vindana, K. Vencatasamy, K.V. Lawler, A. Salamat, R.P. Dias, Room-temperature superconductivity in a carbonaceous sulfur hydride, Nature 586 (2020) 373–377.

[7] A.W. Sleight, J.L. Gillson, P.E. Bierstedt, High-temperature superconductivity in the $BaPb_{1-x}Bi_xO_3$ systems, Soli. Stat. Commun. 17 (1975) 27–28.

[8] R.J. Cava, B. Batlogg, J.J. Krajewski, R. Farrow, L.W. Rupp, A.E. White, K. Short, W.F. Peck, T. Kometani, Superconductivity near 30 K without copper: the $Ba_{0.6}K_{0.4}BiO_3$ perovskite, Nature 332 (1988) 814–816.

[9] L.F. Mattheiss, E.M. Gyorgy, D.W. Johnson, Superconductivity above 20 K in the Ba–K–Bi–O system, Phys. Rev. B 37 (1988) 3745–3746.

[10] D.G. Hinks, B. Dabrowski, J.D. Jorgensen, A.W. Mitchell, D.R. Richards, S. Pei, D. Shi, Synthesis, structure and superconductivity in the $Ba_{1-x}K_xBiO_{3-y}$ system, Nature 333 (1988) 836–838.

[11] S. Nakamura, Y. Koyama, M. Ishimaru, Structural transitions in $Ba_{1-x}M_xBiO_3$ (M = K, Rb), Physica C 185-189 (1991) 695–696.

[12] S. Pei, J.D. Jorgensen, B. Dabrowski, D.G. Hinks, D.R. Richards, A.W. Mitchell, J.M. Newsam, S.K. Sinha, D. Vaknin, A.J. Jacobson, Structural phase diagram of the $Ba_{1-x}K_xBiO_3$ system, Phys. Rev. B: Cond. Mat. 41 (1990) 4126–4141.

[13] M.L. Norton, Electrodeposition of $Ba_{0.6}K_{0.4}BiO_3$, Mater. Res. Bull. 24(11) (1989), 1391–1397.

[14] S.N. Barilo, S.V. Shiryaev, V.I. Gatalskaya, J.W. Lynn, M. Baran, H. Szymczak, R. Szymczak, D. Dew-Hughes, Scaling of magnetization and some basic parameters of $Ba_{1-x}K_xBiO_{3+y}$ superconductors near T_c, Phys. Rev. B 58 (1998) 12355–12367.

[15] L.A. Klinkova, M. Uchida, Y. Matsui, V.I. Nikolaichik, N.V. Barkovskii, Noncubic layered structure of $Ba_xK_{1-x}BiO_3$ superconductor, Phys. Rev. B 67 (2003) 140501.

[16] C. Yajing, C. Yongliang, C. Cuihua, C.C. Sorrell, Z. Yong, Effects of La- and Pr-Substitution on the Structure and Superconductivity of $Ba_{0.6}K_{0.4}BiO_3$, Rare Metal Mat. Eng. 44(9) (2015) 2081–2085.

[17] R. Bezzenberger, R. Schöllhorn, Electrochemical synthesis of perovskite type oxobismuthates (III/V) from hydroxide melts, Eur. J. Solid State Inorg. Chem. 30 (1993) 435–445.

[18] G.M. Zhao, D.E. Morris, Composition dependence of the oxygen isotope effect in $Ba_xK_{1-x}BiO_3$: Evidence for oxygen-mass dependence of the coupling constant, Phys. Rev. B 51 (1995) 12848–12851.

[19] W.D. Mosley, M.D. Lan, P.A. Sterne, R.H. Howell, R.N. Shelton, Correlation of magnetic properties to oxygen and potassium stoichiometry in single-crystal $Ba_{1-x}K_xBiO_{3-y}$, J. Superconduc. 7 (1994) 299–301.

[20] D.C. Kim, A.N. Baranov, J.S. Kim, H.R. Kang, B.J. Kim, Y.C. Kim, J.S. Pshirkov, E.V. Antipov, Y.W. Park, High pressure synthesis and superconductivity of $Ba_{1-x}K_xBiO_3$ ($0.35 < x < 1$), Physica C 383 (2003) 343–353.

[21] A.P. Menushenkov, K.V. Klementev, Extended X-ray absorption fine-structure indication of a double-well potential for oxygen vibration in $Ba_{1-x}K_xBiO_3$, J. Phys.: Cond. Mat. 12 (2000) 3767–3786

[22] K. Foyevtsova, A. Khazraie, I. Elfimov, G.A. Sawatzky, Hybridization effects and disproportionation in the bismuth perovskites, Phys. Rev. B 91 (2015) 121114(R).

[23] Y. Idemoto, Y. Iwata, K. Fueki, Defect chemistry of $Ba_{1-x}K_xBiO_y$ superconductors, Physica C 222 (1994) 257–266.

[24] H.K. Liu, S.X. Dou, K.H. Song, C.C. Sorrell, K.E. Easterling, W.K. Jones, Cu valence states in superconducting Bi-Pb-Sr-Ca-Cu-O system, J. Soli. Stat. Chem. 87 (1990) 289–297.

[25] D. Telesca, Y. Nie, J.I. Budnick, B.O. Wells, B. Sinkovic, Impact of valence states on the superconductivity of iron telluride and iron selenide films with incorporated oxygen, Phys. Rev. B 85 (2012) 214517.

[26] W.R. Pudełko, A. Krztoń-Maziopa, A. Lynnyk, R. Puźniak, K. Ławniczak-Jabłońska, D.J. Gawryluk, D. Moszczyńska, J. Mizera, Bismuth and oxygen valencies and superconducting state properties in $Ba_{1-x}K_xBiO_3$ superconductor, Physica B: Phys. Cond. Mat. 591(41) (2020) 412226.

[27] Y.J. Uemura, B.J. Sternlieb, D.E. Cox, J.H. Brewer, R. Kadono, J.R. Kempton, R.F. Kiefl, S.R. Kreitzman, G.M. Luke, P. Mulhern, T. Riseman, D.L. Williams, W.J. Kossler, X.H. Yu, C. E. Stronach, M.A. Subramanian, J. Gopalakrishnan, A.W. Sleight, Absence of magnetic order in (Ba, K)BiO_3, Nature 335 (1988) 151–152.

[28] B. Batlogg, R.J. Cava, L.W. Rupp Jr., A.M. Mujsce, J.J. Krajewski, J.P. Remeika, W.F. Peck Jr., A.S. Cooper, G.P. Espinosa, Density of States and Isotope Effect in BiO Superconductors: Evidence for Nonphonon Mechanism, Phys. Rev. Lett. 61 (1988) 1670–1673.

[29] S. Kondoh, M. Sera, Y. Ando, M. Sato, Normal state properties and oxygen isotope effect of (Ba, K)BiO_3, Physica C 157 (1989) 469–477.

[30] K. Motizuki, M. Shirai, The role of electron-phonon interaction in oxide superconductors, Physica B 186-188 (1993) 816–821.

[31] L.F. Mattheiss, D.R. Hamann, Electronic structure of $BaPb_{1-x}Bi_xO_3$, Phys. Rev. B 28 (1983) 4227–4241.

[32] L.F. Mattheiss, D.R. Hamann, Electronic Structure of the High-T_c Superconductor $Ba_{1-x}K_xBiO_3$, Phys. Rev. Lett. 60 (1988) 2681–2684.

[33] G.M. Eliashberg, Interactions between electrons and lattice vibrations in a superconductor, Sov. Phys. JETP 11(3) (1960) 696–702.

[34] G.M. Eliashberg, Temperature Green's function for electrons in a superconductor, Sov. Phys. JETP 12(5) (1961) 1000–1002.

[35] R. Kim, J. Yu, H. Jin, Graphene analogue in (111)-oriented $BaBiO_3$ bilayer heterostructures for topological electronics, Sci. Rep. 8(1) (2018) 555.

[36] R. Vidyasagar, B. Camargo, E. Pelegova, K. Romanyuk, A.L. Kholkin, Controlling Surface potential of graphene Uuing dc electric field, ASRTU Conference Proceedings - IV Sino-Russian ASRTU Symposium on Advanced Materials and Processing Technology 2016 (2016) 183–189.

[37] M.L. Norton, H.Y. Tang, Superconductivity at 32 K in electrocrystallized Ba-K-Bi-O, Chem. Mat. 3(3) (1991) 431–434.

[38] R.J. Cava, B. Batlogg, J.J. Krajewski, R. Farrow, L.W. Rupp, A.E. White, K. Short, W.F. Peck, T. Nishio, H. Minami, U. Uwe, Large single crystals of $Ba_{1-x}K_xBiO_3$ grown by electrochemical technique, Physics C: Superconductivity and its applications 332 (357-360) (2001) 376–379.

[39] P.D. Han, L. Chang, P.A. Payne, Top-seeded growth of superconducting $(Ba_{1-x}K_x)BiO_3$ crystals by an electrochemical method, J. Crystal Growth 128 (1993),798–803.

[40] M.E. Tittlebaum, W.R. Lea, Potential environmental impact of phosphogypsum in stockpiles and certain commercial applications, Report I-90-5, Institute of Recyclable Materials, Louisiana State University, December 1990, 18.

[41] P.A. Kolniak, Synthesis and physical characterization of solid-state materials, Louisiana State University (1988), dissertation, as of the day 1st April 2021: https://digitalcommons.lsu.edu/gradschool_disstheses/6684.

[42] S. Kodialam, V.C. Korthius, R.D. Hoffmann, A.W. Sleight, Electrodeposition of potassium bismuthate: $KBiO_3$, Mater. Res. Bull. 27 (1992) 1379–1384.

[43] G.L. Roberts, S.M. Kauzlarich, R.S. Glass, J.C. Estill, Investigation of the mechanism of electrosynthesis of the superconductor, barium potassium bismuth oxide ($Ba_{1-x}K_xBiO_3$), Chem. Mater. 5(11) (1993) 1645–1650.

[44] J. Rodriguez-Carvajal, Recent advances in magnetic structure determination by neutron powder diffraction, Physica B 192 (1993) 55–69.

[45] R. Gautam, S. Vanga, F. Ariese, S. Umapathy, Review of multidimensional data processing approaches for Raman and infrared spectroscopy, EPJ Tech. Instrument. 2(8) (2015) 1–38.

[46] J.H. Ward, Hierarchical grouping to optimize an objective function, J. Am. Statistic. Assoc. 58, 1963, 236–244.

[47] P. Giannozzi, S. Baroni, N. Bonini, M. Calandra, R. Car, C. Cavazzoni, D. Ceresoli, G.L. Chiarotti, M. Cococcioni, I. Dabo, A. Dal Corso, S. de Gironcoli, S. Fabris, G. Fratesi, R. Gebauer, U. Gerstmann, C. Gougoussis, A. Kokalj, M. Lazzeri, L. Martin-Samos, N. Marzari, F. Mauri, R. Mazzarello, S. Paolini, A. Pasquarello, L. Paulatto, C. Sbraccia, S. Scandolo, G. Sclauzero, A.P. Seitsonen, A. Smogunov, P. Umari, R.M. Wentzcovitch, QUANTUM ESPRESSO: a modular and open-source software project for quantum simulations of materials, J. Phys.: Cond. Mat. 21(39) (2009) 395502.

[48] P. Giannozzi, O. Andreussi, T. Brumme, O. Bunau, M. Buongiorno Nardelli, M. Calandra, R. Car, C. Cavazzoni, D. Ceresoli, M. Cococcioni, N. Colonna, I. Carnimeo, A. Dal Corso, S. de Gironcoli, P. Delugas, R.A. DiStasio Jr., A. Ferretti, A. Floris, G.

Fratesi, G. Fugallo, R. Gebauer, U. Gerstmann, F. Giustino, T. Gorni, J. Jia, M. Kawamura, H.-Y. Ko, A. Kokalj, E. Küçükbenli, M. Lazzeri, M. Marsili, N. Marzari, F. Mauri, N.L. Nguyen, H.-V. Nguyen, A. Otero de la Roza, L. Paulatto, S. Poncé, D. Rocca, R. Sabatini, B. Santra, M. Schlipf, A.P. Seitsonen, A. Smogunov, I. Timrov, T. Thonhauser, P. Umari, N. Vast, X. Wu, S. Baroni, Advanced capabilities for materials modeling with Quantum ESPRESSO. J. Phys.: Cond. Mat. 29(46) (2017) 465901.

[49] D.T. Marx, P.G. Radaelli, J.D. Jorgensen, R.L. Hitterman, D.G. Hinks, S. Pei, B. Dabrowski, Metastable behavior of the superconducting phase in the $BaBi_{1-x}Pb_xO_3$ system, Phys. Rev. B 46 (1992) 1144–1156.

[50] M. Braden, W. Reichardt, E. Elkaim, J.P. Lauriat, S. Shiryaev, S.N. Barilo, Structural distortion in superconducting $Ba_{1-x}K_xBiO_3$, Phys. Rev. B 62 (2000) 6708–6715.

[51] S. Pei, J.D. Jorgensen, D.G. Hinks, Y. Zheng, D.R. Richards, B. Dabrowski, A.W. Mitchell, Structure and chemistry of $Ba_{0.6}K_{0.4}BiO_y$ at high temperature, J. Solid State Chem. 95, (1991) 29–38.

[52] M. T. Weller, J.R. Grasmeder, P.C. Lanchester, P.A.J. de Groot, G.P. Rapson, A.C. Hannon, The structure and superconducting properties of $Ba_{0.7}K_{0.3}BiO_{2.91}$, Physica C 156 (1988) 265–268.

[53] L.F. Schneemeyer, J.K. Thomas, T. Siegrist, B. Batlogg, L.W. Rupp, R.L. Opila, R.J. Cava, D.W. Murphy, Growth and structural characterization of superconducting $Ba_{1-x}K_xBiO_3$ single crystals, Nature 335 (1988) 421–423.

[54] Z. Schlesinger, R.T. Collins, J.A. Calise, D.G. Hinks, A.W. Mitchell, Y. Zheng, B. Dabrowski, N.E. Bickers, D.J. Scalapino, Superconducting energy gap and a normal-state excitation in $B_{0.6}K_{0.4}BiO_3$, Phys. Rev. B 40(10) (1989) 6862–6866.

[55] R. Das, A. Midya, M. Kumari, A. Chaudhuri, X. Yu, A. Rusydi, R. Mahendiran, Enhanced magnetocaloric effect driven by hydrostatic pressure in Na-doped $LaMnO_3$, J. Phys. Chem. C 123(6) (2019) 3750–3757.

[56] J. Yang, T. Xie, Ch. Liu, L. Xu, Facile Fabrication of Dumbbell-Like β-Bi_2O_3/Graphene Nanocomposites and Their Highly Efficient Photocatalytic Activity, Materials 11(8) (2018) 1359.

[57] S. Koçyiğit, Ö. Gökmen, S. Temel, A. Aytimur, İ. Uslu, S. H. Bayari, Structural investigation of boron undoped and doped indium stabilized bismuth oxide nanoceramic powders, Ceram. Int. 39(7) (2013) 7767–7772.

[58] J.E. Graebner, L.F. Schneemeyer, J.K. Thomas, Heat capacity of superconducting $Ba_{0.6}K_{0.4}BiO_3$ near T_c, Phys. Rev. B 39(13) (1989) 9682–9684.